Concurrent saliency and intentional maps in posterior parietal cortex

Ruichen Zheng[1,2,3], Yong Gu[1,3*] and He Cui[1,2*]

1 Center for Excellence in Brain Science and Intelligence Technology, Institute of Neuroscience, Chinese Academy of Sciences, Shanghai 200031, China

2 Chinese Institute for Brain Research, Beijing, 102206, China

3 University of Chinese Academy of Sciences, Beijing 100049, China

* Corresponding authors

Email: hecui@cibr.ac.cn

Abstract

The goal for the motor action represents the desired state of the individual to interact with world. Investigating how the goal is generated requires clarifying spatial extrapolation that involves perceptual and action processes. Here, we recorded neural activity from monkeys manually intercepting a circularly moving target being occluded. The saliency and intentional maps, which developed to locate the target of interest and the intended action goal, were thus distinguished in neural activity recorded from the lateral intraparietal cortex (LIP) and parietal reach region (PRR). Dynamic internal representations spanning from visual registration to state estimation were unveiled in both areas, with the goal for the interception being inferred as the visual consequence of the movement. The motion extrapolation was found to be an intrinsic part of movement planning so that the continuous and stable spatial extrapolation from motion to action was prevalent in both areas. The goal estimation based on the sensory extrapolation rationalized the concurrency and correlation of saliency and intentional maps, which were found to switch their dominance by reorganizing the read-out dimensions of the spatial manifold. The extrapolation achieved at both the perceptual and motor stages not only bridged the saliency and intentional maps, but also revealed the form of the state estimation in guiding predictive sensorimotor control.

Introduction

Animals live in an ever-changing environment while physical delays in the nervous system cannot be eliminated solely through biophysical improvement. To interact with dynamic world, the nervous system could direct the individual to act toward the future, compensating delays in the motor stage, as a predator intercepts the prey (Mischiati, 2015), or specifically regarding primates operating or intercepting a moving object (Flanagan et al., 2001; Zago et al., 2004). Since the flag-lag effect has been observed under various conditions (Nijhawan, 1994; Sheth, Nijhawan, and Shimojo, 2000; Alais and Burr, 2003), whether the motor compensation is sufficient for behavior construction has been discussed. As two forms of interaction between the individual and environment, action and perception are argued to be served by the separated pathways. If both processes require predictive compensation, identifying the spatial extrapolation they share could be essential in revealing how the motor action was planned.

Controversies surrounding the predictive compensation mirror the discussion about the signal embedded in the posterior parietal cortex (PPC), where extrapolation related to both sensory stimuli and motor consequence has been observed (Assad and Maunsell, 1995; Eskandar and Assad, 1999; Duhamel, Colby, and Goldberg, 1992; Mulliken, Musallam, and Andersen, 2008). As a crucial sensorimotor interface, the PPC has long been deliberated to integrate signals from multiple sources to develop a spatial map that locates behavior-relevant motor apparatus and

external items, referred to as the intentional map and saliency map, respectively (Andersen and Cui, 2009; Bisley and Goldberg, 2010). The task-dependent literal-to-abstract activity raises rich frameworks centered on action- or perception-oriented processing. However, the design of conventional tasks caused the motor action to always be directed to predefined sensory cues, the signal reflecting existing stimuli and action goals was thus difficult to distinguish.

In recent studies, a manual interception task was designed to dissociate neural tuning to instantaneous stimulus and upcoming movement (Li, Wang, and Cui, 2018), revealing that pre-movement activity in area 7a was found to be co-varied with the reach direction instead of target location (Li, Wang, and Cui, 2022). In contrast, motor cortical activity was strongly modulated by target motion (Zhang, Chen, et al., 2024) and is involved in continuous sensorimotor transformations (Zheng, Wang, and Cui, 2025). Nevertheless, it remained unclear how predictive signal emerges and whether it indeed encodes motion extrapolation or action goal. In the present study, we modified the interception task by occluding the target for a fixed period after cue presentation, allowing the movement to be prepared without tracking the target. Our recording from the lateral intraparietal area (LIP) and the parietal reach region (PRR) showed that interceptive movement was planned in the form of visual extrapolation concerning target motion to movement consequences. The absence of visual input emphasized the concurrent motion extrapolation and goal estimation, suggesting that sensory extrapolation is integral to action planning. Our results suggested the coexistence of the saliency and intentional maps and transition from the former to the latter, which was achieved by exploiting different dimensions of neural state space. Therefore, seemingly contradictory attention/saliency versus intention/decision models might be reconciled under the continuous sensorimotor transformation, revealing the circuit involving PPC that converges perception and action stages.

Results

Behavior

Two rhesus monkeys were trained to make a reaching movement towards a moving or stationary target while maintaining gaze fixation throughout a trial (Figure 1A). The beginning of a trial was marked by the fixation of the gaze and the hand at the center of the screen. When the Fixation lasted for a while (400 ms), a target appeared (Cue on) and moved circularly around the center or remained static. The location of the target was presented to the monkeys during the Cue period for a variable duration (400-800 ms), then absent (Cue off) during the remainder of the trial. After the target was invisible for a fixed Occlusion period (500 ms), the monkeys were free to touch the target as the fixation point was darkened (Go), and received feedback when the reaching movement was completed.

The initial direction and the motion velocity of the target, as well as the duration of the Cue, were selected pseudo-randomly in each trial. Therefore, the movement was planned largely based on the target information acquired in the current trial. The adaptable mapping between the target and the movement led to a relatively uniform distribution of reach endpoints (Figure 1B), except that the upper region was relatively less touched due to the experimental apparatus and limb posture. The endpoints did not cluster into certain zones, and were distributed around the target without a significant undershoot or overshoot (the distribution of motor error, i.e., difference between the endpoint and the target position, was deviated from zero distribution less than 1 degree without velocity dependence), suggesting that the monkeys have not developed the habit of intercepting only at preferred regions. The urgency difference between the conditions with moving and stationary target (Figure S1, t-test, $p < 0.001$), manifested as shorter reaction time and movement duration in the interceptive movement, also implied that the monkeys performed interception with little hesitation.

Intercepting a moving target after a considerable period without available visual information is challenging. After extensive training, the interceptive movement of monkey subjects always predictively aimed at the target location at the end of the movement, but did not behave as a habitual movement towards fixed regions. The anticipation required for a successful trial and the flexible relationship between the target and the planned movement in the interception task make it advantageous to investigate the neuronal response to the visual stimulus and the impending movement.

Dissociated stimulus and movement modulation in neural responses

Task-related modulation of individual neurons could be described by a tuning curve that specifies the relation between the neuronal activity and the target or movement direction. Benefit from the dynamic visual input and self-initiated movement, organizing the trials according to the instantaneous target direction to fit the directional tuning curves would shuffle the reach direction of corresponding trials, and vice versa. Therefore, at a certain moment, the tuning curves defined by the instantaneous target direction would be aligned across five velocity conditions if a neuron responded to the stimulus, and would be shifted with velocity when defined by the reach direction; conversely, a neuron responding to the movement would demonstrate consistent movement tuning curves and disordered stimulus tuning curves (Figure 1C).

Neurons were recorded from LIP and PRR separately; the well-isolated units that displayed task relevance (see Electrophysiology) were included for further analysis (LIP: 86 and 245 for monkey A and monkey N, with single-electrode and linear probes, respectively; PRR: 65 and 294 for monkey A and monkey N, respectively; Figure 1D). In accordance with previous studies involving sensory-guided movement, neurons in LIP and PRR always discharged for a varying period after the stimulus-evoked response. As shown in Figure 2, two example neurons recorded from LIP

and PRR, respectively, exhibited a rapid elevation in activity following Cue on, and a distinct development of persistent activity as Go approached.

Activity in both areas appeared to be contingent on the target or intended movement during different periods (Figure S1, S2). Identifying the stimulus- and movement-related signals by directional tuning is consequently essential to reveal the potential representation transition underlying the persistent activity. As exemplified by the two types of tuning around the three task events (Figure 2B and 2D), the vigorous responses triggered by the visual stimulus was reliably tuned to the target across conditions, verifying the stimulus modulation at 0.2 s after Cue on in both example neurons. When the target was masked, the directional tunings diverged between the two neurons. The tuning curves of the LIP neuron were more aligned with the target than the reach direction, while those of the PRR neuron were consistently directed to the reaching movement at both Cue off and Go, indicating an attenuated stimulus modulation and a robust movement modulation in the two neurons, respectively.

Gradient directional tunings from stimulus to movement

By comparing the stimulus- and movement-defined directional tunings, the time-varying representation preference of each neuron could be assessed. A sensorimotor index, which was defined according to the variance of two types of directional tunings, was computed to measure the tendency to represent stimulus and movement by a value ranging from -1 to 1. For instance, the index of the two example neurons at 0.2 s after Cue on was -0.9, indicating a strong stimulus modulation; during the Occlusion, the gradually weakened stimulus modulation in the LIP neuron was signified by the index of -0.7 and -0.4, and the constant movement modulation in PRR neuron were signified by the index of 0.8 and 0.9 respectively at Cue off and Go.

From Cue on to Go, the distributions of the index derived from LIP and PRR neurons over different epochs are illustrated in Figure 3A. As shown by distributions in six example time windows, the median of the distribution shifted from negative to positive in both populations, suggesting an overall transition from stimulus coding to movement coding in the populations. Additionally, the index of LIP neurons was always significantly lower than that of PRR neurons (time windows labeled with an asterisk, Wilcoxon rank sum test, $p < 0.001$), suggesting that LIP neurons were more likely to be modulated by the stimulus than PRR neurons.

Does the population-level change of the sensorimotor index result from the separate activation of neurons exclusively responding to the stimulus and the movement? For the neurons demonstrating sustained directional selectivity, the shift of the index was denoted as a vector determined by the first and last index in the direction-sensitive period. Distribution of the shift vectors primarily consisted of the sector directing 135°, which included most of the neurons in two areas, and the sector directing 180°, which was also considerable in the LIP, revealing the subpopulations involved in sensorimotor transformation and sensory processing, respectively

(Figure 3B and 3C). Notably, shift vectors are predominantly distributed on the left half of the coordinate axes, implying that the neurons modulated by the movement typically underwent stimulus modulation (i.e., the direction-sensitive period always started from a negative index). Irrespective of the evolvement of persistent activity, nearly half of the LIP and PRR neurons modulated by the direction were recruited in representing both the target and the imminent reach, confirming the engagement of the two populations in sensory-guided movement. Before the movement was executed, it could be inferred where to reach as soon as the task entered the period which planning was allowed. Such inference often followed representation for the target, suggesting a sequential extrapolation from visual motion to movement consequence. However, as the neurons experiencing the transformation accumulated, the variance in directional tunings was also found to increase, implying that the transformation process was not synchronized among neurons.

Courses of tuning state transition

In the gradient from stimulus tuning to movement tuning, some neurons seemed not to be exactly tuned to the instantaneous stimulus or the final movement (for example, the directional tunings in Figure 2B during the Occlusion), raising the question of whether the neurons simply track the actual target when they respond to it.

To uncover the detailed process of representation, the lack of explainability of the current target and intended movement was investigated by testing a set of directional variables expressed as the sum of the instantaneous target direction and a deviation angle. The deviation angle is defined by the motion velocity and a condition-independent response latency “tau”, denoting the spatial difference between the represented and the current state of the target. A negative “tau” signifying a neuron response to the current target with latency, and a positive “tau” signifying a neuron response to the current target in advance. For each time bin, the variables including target states with tau ranging from -0.9 s to 0.9 s with step of 0.05 s and the reach direction were all tested to identify which best explained the directional selectivity of a single neuron. Again, the alignment of the tunings defined by the tested variables across conditions and R-square was used to evaluate the goodness of explanation. The tested variable that maximizes the tuning alignment and R-square was defined as the tuning state. Fitting the firing rates by the tuning state significantly improved the R-square (Figure S4, t-test, $p < 0.001$), confirming that the tuning state was the most probable object to which a neuron was tuned.

Figure 4 shows the tuning states of the example neurons. As suggested by the above comparison of stimulus and movement tunings, the PRR neuron in Figure 2 tracked the target with minimal latency during the Cue, and persistently represented the intended movement during the Occlusion (Figure 4B). Such a transition was also observed in LIP neurons (Figure 4C), revealing the predictive compensation concerning both sensory and motor delays at the level of the

individual neuron. Other forms of motion extrapolation were also remarkable; for example, it could be generalized to situations where the visual input was blocked (Figure 4D), accumulated over time (Figure S5A), or maintained stable over-extrapolation (Figure S5B). Delayed visual registration, with or without updating, was kept as well (Figure 4A, S5C). An assortment of tuning state developments suggested a dynamic pool converging salience and intention at different timescales in both LIP and PRR.

Availability of multiple internal estimation in the populations

It is not easy to summarize the transition of the tuning state into specific patterns. Therefore, we first classified the tuning states into four categories according to their temporal relationship with the actual target: the lagging target state with the tau less than or equal to -0.1 s; the instantaneous target state with the tau between -0.1 and 0.1 s; the leading target state with the tau greater than or equal to 0.1 s, but not equivalent to the movement; and the intended movement. The distribution of tuning states across two populations is shown in Figure 5A and 5C. In both LIP and PRR, the instantaneous and the lagging states were prevalent during the Cue. As the Cue approached the end, increasingly neurons extrapolated the target states into the near future. After Cue off, the leading state and the movement then became dominant, which was more evident in PRR. The instantaneous motion extrapolation still lasted in the early Occlusion, while the delayed motion information was preserved in a small portion of neurons, which was more common in LIP.

Next, a set of support vector machine regression models (rSVMs) was constructed to examine the read-out of tuning states from population activity. The rSVM for each time bin was trained by the activity and direction labels interpolated by the instantaneous tuning function of each neuron and tested with real data. The performance for decoding two lagging target states (tau = -0.2 s, -0.4 s), the instantaneous target states (tau = 0), two leading target states (tau = 0.2 s, 0.4 s), and the intended movement was chosen as examples for demonstration (Figure 5B, 5D). Parallel to the distribution of the tuning states, the rSVMs of both areas acquired from the Cue performed well in decoding the location of the instantaneous and lagging target, as well as the leading target. The reach direction was barely decoded from the population activity until the Cue off. During the Occlusion, the accuracy in decoding the movement underwent a gradual and sharp rise in LIP and PRR, respectively, while the accuracy in decoding the instantaneous and leading target remained at a high level. For comparison, decoding the lagging target was no longer as easy as that during the Cue, especially in PRR.

The tuning states in LIP and PRR demonstrated high flexibility under task restriction, while neurons in LIP registered the target-related salience for a longer period, and neurons in PRR started to figure out the action goal earlier. The availability of visual information facilitated the internal representation to match the actual state of the target; then the visual extinction prompted

226 the simulation regarding both the motion and movement prevalent across neurons, emphasizing
227 the role of the two areas in the sensorimotor control.

228 **Reorganization of the potent spatial map underlying sensorimotor transformation**

229 Tuning states changed at dissimilar pace in single neurons, which benefits selective read-out
230 over a broader range. Considering the sensorimotor transformation necessarily implicated
231 network computation, the dynamic tuning states could be a manifestation of the ongoing
232 computations. However, the directional selectivity, which was determined by the connections, did
233 not undergo significant changes over a short period of time (Figure S6), raising the question of
234 how the populations modified the internal representation without extensively altering the spatial
235 map.

236 Time-varying response patterns may enable the spatial map of the population to support assorted
237 internal representations. To explore this possibility, the activity organized by the tuning functions
238 (i.e., tuning matrix) acquired above was transformed into a combination of a set of principal
239 components (PCs) in virtue of the principal component analysis (PCA). As shown in Figure 6A
240 and 6C, the spatial map of the LIP and PRR manifests as a ring consisting of the neural states
241 occupying directions on a circle in the low-dimensional space. As the task proceeded, the rings
242 colored from blue to green rotated in the state space, demonstrating an invariant spatial map in
243 the first two dimensions and a reorganization in the third dimension.

244 Next, the subspaces related to the stimulus and movement were estimated. One was acquired
245 from the stimulus matrix, encompassing the population activity during the early Cue (from 0.05 s
246 to 0.3 s after Cue on) and organized with instantaneous target direction; the other was acquired
247 from the movement matrix, encompassing the population activity during the late Occlusion (from
248 0.25 s to 0.5 s after Cue off) and organized with reach direction. After performing PCA on the two
249 matrices, the stimulus and movement data were projected onto each resulting subspace. The
250 stimulus PCs captured little variance of the movement-related activity, and the movement PCs
251 captured little variance of the stimulus-related activity (Figure S7, according to Elsayed et al.,
252 2016), suggesting the near orthogonality between the stimulus and movement PCs.

253 With the tuning matrix projected onto the stimulus and movement PCs, we expected that the
254 projections would be active in the dimensions of stimulus subspace during the Cue, and active in
255 the dimensions of movement subspace during Occlusion. Interestingly, the projections onto both
256 subspaces were active during the Cue. Trajectories in each direction unfolded following Cue on,
257 then folded back in the stimulus subspace and continuously spread in the movement subspace
258 (Figure 6B, 6D). When visualizing the evolution of neural states in the space spanned by the first
259 two stimulus dimensions and the first movement dimension, the transition of the dimensions
260 where the neural states evolved was evident (Figure 6E).

Together with the similar activity variance explained by the stimulus and movement PCs (Figure 6F), it could be speculated that the spatial map locating the behavior-relevant visual stimulus and the motor goal actually overlap instead of being exclusive in the populations. Switch of the representation could be achieved by exploiting different dimensions of the neural state space, which was driven by the dynamics of population activity. Therefore, the development of motion extrapolation and motor planning could be a correlated and flexible process.

Disscussion

How are perception and action guided under evolving circumstances? In the present study, we designed the occluded manual interception task to prompt the motor action generated in a feedforward way, disassociating the visual motion and motor goal in the neural representation. A dynamic pool involving visual memory, inferred target motion, and reach planning was observed in both LIP and PRR, with the primary difference between the two areas reflected in the ratio of representations in the populations. The diverse transition from saliency to intentional map was then clarified. Such transitions suggested abundant readout and dynamics in the population activity, which was found to drive the reorganization of the spatial manifold in the neural state space. These findings revealed the associated spatial maps that located the behavior-relevant cue and goal prospectively, demonstrating the engagement of the PPC in a generalized internal model benefiting both perception and action.

Constructing proactive motor behavior relies on the estimation of motor consequence, which is known as a forward model (Jordan and Rumelhart, 1992; Wolpert, Ghahramani, and Jordan, 1995), proposed as a solution to overcome the inevitable delay in action generation. Based on the estimation, the effector could be displaced to the location where the external object will be at the movement offset. Simulations for both the object and the effector are thus required. The inferred target motion could be conveyed by LIP activity (Assad and Maunsell, 1995; Eskandar and Assad, 1999, 2002), and the modulation of stimulus motion has been broadly observed in retina ganglion cells (Berry et al., 1999), optic tectum (Witten, Bergan and Knudsen, 2006), V1 (Subramaniyan et al., 2018), and V4 (Sundberg, Fallah and Reynolds, 2006). The signal that routes the efference copy of motor command to modulate sensory processing has been observed across species (Crapse and Sommer, 2008), which specifically manifests as remapping of the receptive field (Duhamel, Colby and Goldberg, 1992; Batista et al., 1999), or real-time tracking of effector (Mulliken, Musallam and Andersen, 2008) in the PPC. However, spatial extrapolation regarding the interaction between object and effector has not been explicitly addressed, although the temporal prediction (Lee, 1976) has been widely investigated under the simplified interceptive movement that the interception zone was pre-determined (Port et al., 2001; Merchant, Battaglia-Mayer, and Georgopoulos, 2001, 2003). As in the case of the occluded interception task, a

successful interceptive movement was planned by tracking and predicting the target motion in accordance with limb movement, rendering goal specification to rely on internal prediction instead of artificially defined rules.

The spatial extrapolation concerning target motion and motor consequence was carried out in both LIP and PRR. Noticeably, the intended movement was always represented following motion representation, suggesting the correlated extrapolation from motion to movement. The early proposition of internal model emphasized the state estimation for the motor apparatus (Wolpert, Ghahramani, and Jordan, 1995; Wolpert and Flanagan, 2001), that is, the delays in sensory processing and movement execution could be compensated by directing action at the desired state (Kerzel and Gegenfurtner_2003; Purushothaman et al., 2008; Sheth and Wu, 2008). In our task, the fixed duration of the Occlusion made the visual extrapolation no longer unnecessary. Interestingly, visual extrapolation was still observed, while the instantaneous extrapolation that compensated for sensory latency was dominant during the Cue, and the over-extrapolation was dominant during the Occlusion. Although we were incapable of further inspecting whether these visual extrapolations were a mix of the delayed target motion and the inaccurate goal estimation, in the view of holistic internal representation, the state estimation at different time-scales, incorporating both motion and motor extrapolation developed in the two areas, suggests a hierarchical predictive coding (Rao, 2024) involving the PPC.

The saliency and intentional map were established in the PPC (Andersen and Buneo, 2002; Bisley and Goldberg, 2010), which underpinned the role of the PPC in the sensorimotor transformation. The intentional map, used to assign the desired endpoint of a motor plan, is inherently anticipatory. The saliency map, used to convey the interpretation of existing sensory stimuli, seems to be reactive. In the face of dynamic sensory input, the representation regarding the delayed and inferred target motion was found in both LIP and PRR, suggesting parallel saliency maps that were responsible for registering and inferring. These findings extended the scope that the saliency map referred to, that is, the saliency map functions far more than a reactive description.

Whereas a large body of evidence suggests that the PPC is composed of multiple functional subareas with distinct roles in the sensorimotor transformation (Kaas and Stepniewska, 2016; Kaas, Qi, and Stepniewska, 2018), we found that LIP and PRR exhibited modest differences in the manual interception task. The LIP and PRR were generally considered to be saccade- and reach-specific, respectively (Snyder et al. 1997; Cui and Andersen 2007). During reach preparation with gaze restriction, considerable LIP neurons were modulated by forthcoming reaching movement. To examine the potential impacts of the saccadic default plan, the endpoints of the saccades after the trial ended were checked. For both subject monkeys, the directions of

331 the first saccade were rarely correlated with reaching movement (Figure S1C), suggesting that
332 the modulation of intended movement hardly resulted from saccade planning.
333 A recent study suggests that the LIP and PRR were likely to plan the movement in parallel (Kang,
334 Mooshagian, and Snyder, 2024). In the LIP, the reaching movement tuning has been reported in
335 the bimanual movement study (Mooshagiana and Snyder, 2018), and the task required manual
336 operation (Oristaglio et al., 2006; Snyder, Batista, and Andersen, 2000). It is likely that the LIP
337 and PRR plan for the imminent behavior-relevant movement rather than the movement performed
338 immediately, which was also the case during decision making, where the LIP activity ramped to
339 support the ultimate decision but not the intervening eye movements (So and Shadlen, 2022).
340 From the viewpoint of the internal model, if the two areas carry the spatial extrapolation pertaining
341 to the effector and target of interest in different modalities, the effector-specific map doesn't have
342 to be modular, because even movements involving a single effector might have multisensory
343 consequences (Medendorp and Heed, 2019). Therefore, beyond artificially separating the
344 movement involving different effectors, further studies were required to explore the sensorimotor
345 transformation underlying the ecological behavior.
346 As discussed above, the saliency and intentional map could be a synthetic spatial manifestation
347 of the behavioral requirement. Considering the abundant connections within the parietal-frontal
348 network, especially the asymmetric projections within the LIP (Ahmed et al., 2025), the saliency
349 and intentional map are expected to be concurrent and correlated when the PPC fulfills the goal
350 of forward prediction in sensorimotor transformation. In the present results, sensorimotor
351 transformation appeared not to be implemented by sequentially activating separate subgroups
352 solely responsible for sensory processing and movement planning, or modified the basic direction
353 selectivity to track the represented object, implying that the saliency and intentional map may
354 share a common spatial map. It could be reasonable at the population level, since sensorimotor
355 transformation needs network computations, while the connections of the networks would not
356 change in a short period. Under the task involving dynamic sensory input and flexible motor
357 output, the sensorimotor transformation was found to be more like a process that defines the
358 spatial map by changing the read-out dimensions. A neuron "possesses" direction selectivity, or
359 the receptive field, before it is specified by task parameters. In the neural state space spanned by
360 the populations, there could be a set of circuits that represent different objects by exploiting
361 different dimensions. The dynamics of population activity was less reported in the studies of the
362 PPC. In recent years, as the dimensionality of behavioral tasks grows, the dynamics in PPC
363 neurons have also become noticeable (Michaels et al., 2015; Michaels et al., 2018; Diomedi et
364 al., 2021). LIP and PRR neurons exhibited heterogeneity during the occluded interception task,
365 which led to the rotation of the spatial manifold in the state space. The projections of the spatial
366 manifold evolved in both stimulus- and movement-related subspace, suggesting an association

367 between the two kinds of map. However, the movement information could be read out only during
368 the Occlusion, suggesting a similar mechanism to the null space hypothesis (Kaufman et al.,
369 2014).
370 As an interface between sensory input and motor output, the converging saliency and intentional
371 maps in the LIP and PRR mediate interaction between individuals and the environment, making
372 the two areas extensively intervene in functions including perception, action, and cognition. In our
373 study, the goal for motor action was found to be generated based on sensory extrapolation that
374 could be the foundation of current perception. How spatial extrapolation is determined by task
375 structures, for example, how the mental tracking and the motor plan evolve when the monkey
376 views the playback, or performs the interception task with a random Occlusion period, is worth
377 further investigation. Furthermore, to address the utility of the spatial extrapolation, the
378 contribution of these extrapolations to behavioral performance, and how the two areas work
379 together, requires further interventional experiments and large-scale simultaneous recordings.

380 **Method**

381 **Experimental model and subject details**

382 Two adult male monkeys (Macaca Mulatta, 7-9 kg and 9-11 kg for Monkey A and Monkey N,
383 respectively) participated in this study. The monkeys performed tasks in the dark and sat in a
384 consumer-designed primate chair with their heads fixed. The titanium (TC4) head post and plastic
385 recording chamber (Crist Instrument, Hagerstown, MD) were implanted stereotaxically by aseptic
386 surgery under isofluorane anesthesia. The location of the head post and chamber was guided by
387 the structural MRI of each monkey. As both monkeys were left-handed, the recording chamber
388 was placed over the intraparietal sulcus (IPS) in the right hemisphere. All training, surgery, and
389 experimental procedures conformed to the National Institutes of Health guidelines and were
390 approved by the Institutional Animal Care and Use Committee (IACUC).

391 **Task design and apparatus**

392 Behavioral tasks were controlled by a computer running Monkeylogic
393 (http://www.monkeylogic.net) under MatLab (version 2018b, MathWorks). The monkeys viewed
394 and interacted with visual stimuli by a touch screen (EloTouch systems Inc., Menlo Park, CA; 100
395 Hz sampling rate, 60 Hz refresh rate), which was placed vertically in front of the monkeys at a
396 distance of 30-40 cm. Gaze position was monitored by an infrared eye tracker (Eyelink 1000 plus,
397 SR Research, Ontario, Canada; 1000 Hz sampling rate). Neural data was recorded by single
398 tungsten electrode (AlphaOmega) and 64-channel S-probe (Plexon Inc.) for monkey A and
399 monkey N, and was collected by AlphaLab SNR (Nazareth, Israel; 22 kHz sampling rate) and
400 Blackrock Microsystems (Cerebus, Salt Lake City, UT; 30 kHz sampling rate), respectively.

In recording sessions, the monkeys performed the occluded manual interception task. To initiate a trial, the monkey was required to foveate and touch the fixation points shown at the center of the screen. After 400 ms, a target was displayed (Cue on) at a random location 14 eccentricity from the center, moved along a circular path with angular velocity randomly selected from 120 °/s clockwise (CW) and counterclockwise (CCW), 200 °/s CW and CCW, or remained stationary. The target was visible to the monkey for 400-800 ms as the Cue period, and was invisible until the monkey touched the screen again. From the target extinguished (Cue off), the monkey kept hand fixation for another 500 ms as the Occlusion period, and was instructed to perform movement by the dimming of the fixation point for the hand (Go). A reach had to be performed within 700 ms (Move), and was considered successful only if the touch endpoint was held within the tolerance window of 7 visual degree from the target for at least 300 ms. The target stopped when the monkey touched the screen, and reappeared with the touch endpoint as visual feedback after the reaching movement was accomplished (Feedback). The endpoint was replaced by a red dot for a successful reach and a blue dot for a failed reach. Following a successful trial ending 500 ms, the monkey was rewarded with a small amount of liquid food. The tolerance window for fixation of gaze and hand was 3 and 5 visual degree from the center points, respectively, and the gaze fixation was restricted until the Feedback ended.

Before or after the recording session, the monkeys were also required to perform mapping tasks that consisted of memory-guided delayed saccade and reach tasks. Both tasks were similar to the condition with stationary target in the interception task, consisting of the Cue period for 500 ms, the Occlusion (Memory) period for 900 ms, the Move period for 700 ms, and the Feedback period for 300 ms. The mapping tasks required the monkey to make eye movement or arm movement to the memorized target according to the color of the target and fixation point, with yellow and green indicating the saccade and the reach, respectively. The gaze was restricted in the reach task, as in the interception task, and the hands were restricted in the primate chair in the saccade task.

Electrophysiology

The activity of well-isolated single units in the lateral intraparietal area (LIP) and parietal reach region (PRR) was recorded using single-channel electrodes and multi-channel linear electrodes for monkey A and monkey N, respectively. 97 recording sessions were conducted in monkey A and 120 in monkey N. In each session, an electrode was directed through a grid to target the lateral or medial bank of the IPS using a motorized microdrive (Thomas Recording GmbH MEM, Giessen, Germany). The subarea to which each recorded neuron belonged was identified in combination with anatomical location and physiological criteria (Andersen, Martyn Bracewell, et al., 1990; Snyder, Batista, and Andersen, 1997). The putative LIP and PRR sites were roughly distributed 3.5-8 mm from subsurface, 2.3–13 mm from midline to lateral, and -10 mm (posterior)

437 to +3.5 mm (anterior) relative to the interaural plane. Neurons with spatial selectivity and that
438 discharged persistently during the mapping tasks were further characterized as LIP or PRR
439 neurons according to the effector preference and were included in the dataset.

440 **Analysis of behavioral data**

441 The monocular position signal was recorded in real-time and was analyzed off-line. The gaze
442 signal was first filtered with a low-pass Butterworth filter to remove the high-frequency noise
443 above 40 Hz. The filtered signal was then smoothed with a 15 ms width rectangular filter. For
444 each trial, the signal in the period from Cue to Feedback was selected to inspect the potential
445 saccades with small amplitude, and the signal in the period from Feedback to Reward was
446 selected to inspect the saccades.
447 After the Feedback, the saccades were detected by the threshold of 30 to 400 eccentricity per
448 second for the horizontal or vertical component. Saccades with a duration of less than 15 ms
449 were excluded, as was the saccade with an amplitude greater than 40 eccentricity (Li, Wang, and
450 Cui, 2018).

451 **Analysis of neuronal data**

452 ***Single neuron analysis***

453 Single units were isolated from the filtered neural signal using Spike2 (v7.15, Cambridge
454 Electronic) for data collected by single-electrode recordings and Kilosort 3.0 (Pachitariu et al.,
455 2016) for data collected by multi-channel recordings.
456 After acquiring the spikes for each unit, the 1 ms-discretized spike train was aligned to Cue on
457 and Cue off, respectively, and was convolved with a Gaussian kernel (δ = 50 ms) to generate the
458 peri-stimulus time histograms (PSTHs). Trial-averaged PSTHs were acquired by averaging the
459 activity from the trials grouped by velocity conditions or direction zones. The standard error was
460 calculated using 10 bootstraps sampled from the corresponding group of trials.
461 For further analysis, the firing rates were calculated for each trial in a 50 ms time window sliding
462 with 25 ms step, and were then standardized by Z-score to ensure that the effect of overall
463 activity fluctuation would not dominate subsequent analyses. After simplifying the visual
464 coordinate to the direction variable, the directional tuning curves were obtained by fitting the firing
465 rates with the direction variables on corresponding trials by the circular version of the Gaussian
466 function:

467 $$r = a + be^{c\cos(\theta-\theta_0)}$$

468 where r is the firing rate in a given time window; a, b, c are coefficients; θ is the direction of the
469 interested variable, which can be the instantaneous target direction or the reach direction, and θ_0
470 is the direction that maximizes the firing rate, i.e. the preferred direction (PD) defined by the
471 interested variable. The directional tuning curves were fitted for each condition, and were filtered

472 by the goodness-of-fit (R-square > 0.1). Given that direction selectivity is considered invariant
473 across conditions, the alignment of directional tunings, as measured by the variance of the PDs
474 or the averaged correlation between the tuning curves, could be used to assess the response
475 preference of a neuron. The preference to respond to the stimulus or the movement was
476 measured by the sensorimotor index, defined as follows:

477 $$index = var(PD_{stim}) - var(PD_{move})/var(PD_{stim}) + var(PD_{move})$$

478 where the PD_{stim} and PD_{move} are PDs defined by the instantaneous target direction and the reach
479 direction, respectively. An index closing to -1 and 1 indicates that a neuron selectively responds
480 to the stimulus and the movement, respectively. The index was calculated only when a neuron
481 showed directional selectivity (the neural responses significantly varied with directions: Kruskal-
482 Wallis test, p < 0.01; R-square of the fitted directional tuning > 0.1). For the neurons displayed
483 directional selectivity for at least 200 ms, the index shift was indicated by a vector whose
484 coordinate was the index at the initial and the end 50 ms of the direction-sensitive period.
485 The variable that modulates the neural activity may not be confined to the current target or the
486 upcoming movement. In this instance, the variable of interest, θ, could be replaced by $\theta_s + \tau v$,
487 where θ_s is the instantaneous target direction, v is the motion velocity, and τ is the condition-
488 independent response latency. The target directions with τ ranging from -0.9 s to 0.9 s with 0.05 s
489 step, as well as the reach direction, were tested to find the variable that was most likely to
490 modulate the neural activity. The directional tunings corresponding to the alternative variables
491 were fitted within and between conditions. The correlation between the tunings fitted under
492 individual conditions, together with the R-square of the tuning fitted across conditions, was used
493 to evaluate the tested variables. The direction variable that maximizes the tuning correlation and
494 R-square was defined as the tuning state, and the corresponding function was defined as the
495 tuning function.

496 ***Population Analysis***

497 To enable the activity of single units to be processed as the population activity recorded
498 simultaneously, the normalized firing rates were interpolated through the tuning function of
499 individual neurons. The interpolated data from each area was then integrated to constitute a
500 tuning matrix with N the number of neurons, C the number of conditions (usually the directions),
501 and T the number of time points.
502 The readout of alternative tuning states from the population activity was examined by the support
503 vector machine regression models (rSVMs) constructed based on the instantaneous tuning
504 functions of each neuron. The training set was the tuning matrix arranged by the direction of
505 tuning states. The direction labels, ranging from 0° to 360° with 10° interval, were transformed
506 into a combination of the horizontal component $x = radius * \cos(\theta)$ and the vertical component
507 $y = radius * sin(\theta)$, where the target path defined the radius. Therefore, two independent

decoders corresponding to each linear component were trained, then tested with real data. The predicted values were converted into directions by the anti-trigonometric function, and the absolute difference between the predicted and the true values was defined as the prediction error to indicate the decoding performance. A permutation test was performed by randomly shuffling the direction labels across trials and recalculating the prediction error 1000 times to acquire the chance level of the rSVMs.

The latent factors in population activity were revealed by transforming the tuning matrix into a set of principal components (PCs) through the standard principal component analysis (PCA). Before the dimension reduction, the mean activity in the dimension of time was subtracted off, and the dimensions of condition were arranged according to tuning directions. The resulting neural states at a given moment were referred to as the spatial map of the population.

The typical task-related dimensions were identified through two other activity matrices which were related to the stimulus and movement, respectively. The former segmented from the population activity during the early 250 ms of the Cue (from 50 ms to 300 ms after Cue on), organized according to instantaneous target direction; the latter segmented from the population activity during the late 250 ms of the Occlusion (from 250 ms to 500 ms after Cue off), organized according to reach direction. The PCs acquired by applying PCA on each matrix were referred to as stimulus and movement PCs, respectively.

For all three subspaces, accumulated variance explained by PCs exceeded 85% of the total by the tenth PC; therefore, the tuning, stimulus, and movement subspaces were defined by the top ten PCs of each. The orthogonality of the stimulus and movement subspaces was quantified according to the variance shared between the two (Elsayed et al., 2016), and the dynamics of the latent factors of population tunings on task-related dimensions was explored by projecting the tuning matrix onto the movement- and stimulus-PCs.

References

Alais, D., Burr, D., 2003. The “flash-lag” effect occurs in audition and cross-modally. Curr. Biol. 13, 59–63. https://doi.org/10.1016/S0960-9822(02)01402-1

Andersen, R.A., Buneo, C.A., 2002. Intentional Maps in Posterior Parietal Cortex. Annu. Rev. Neurosci. 25, 189–220. https://doi.org/10.1146/annurev.neuro.25.112701.142922

Andersen, R.A., Cui, H., 2009. Intention, Action Planning, and Decision Making in Parietal-Frontal Circuits. Neuron 63, 568–583. https://doi.org/10.1016/j.neuron.2009.08.028

Andersen, R.A., Martyn Bracewell, R., Barash, S., Gnadt, J.W., Fogassi, L., 1990. Eye position effects on visual, memory, and saccade-related activity in areas LIP and 7a of macaque. J. Neurosci. 10, 1176–1196. https://doi.org/10.1523/jneurosci.10-04-01176.1990

Assad, J.A., Maunsell, J.H.R., 1995. Neuronal correlates of inferred motion in primate posterior parietal cortex. Nature 373, 518–521.

Batista, A.P., Buneo, C.A., Snyder, L.H., Andersen, R.A., 1999. Reach Plans in Eye Centred Coordinates. Science 285, 257–260. https://doi.org/10.1126/science.285.5425.257

Berry, M.J., Brivanlou, I.H., Jordan, T.A., Meister, M., 1999. Anticipation of moving stimuli by the retina. Nature 398, 334–338. https://doi.org/10.1038/18678

Bisley, J.W., Goldberg, M.E., 2010. Attention, intention, and priority in the parietal lobe. Annu. Rev. Neurosci. 33, 1–21. https://doi.org/10.1146/annurev-neuro-060909-152823

Crapse, T.B., Sommer, M.A., 2008. Corollary discharge across the animal kingdom. Nat. Rev. Neurosci. 9, 587–600. https://doi.org/10.1038/nrn2457

Cui, H., Andersen, R.A., 2007. Posterior Parietal Cortex Encodes Autonomously Selected Motor Plans. Neuron 56, 552–559. https://doi.org/10.1016/j.neuron.2007.09.031

David N. Lee, 1976. A theory of visual control of braking based on information about time-to-collision. Perception 5, 437–459. https://doi.org/10.4324/9780203936672

Diomedi, S., Vaccari, F.E., Galletti, C., Hadjidimitrakis, K., Fattori, P., 2021. Motor-like neural dynamics in two parietal areas during arm reaching. Prog. Neurobiol. 205, 102116. https://doi.org/10.1016/j.pneurobio.2021.102116

Duhamel, J.R., Colby, C.. L., Goldberg, M.E., 1992. The Updating og the Representation of Visual Space in Parietal Cortex by Intended Eye Movements. Science 255, 16–19. https://doi.org/10.1017/CBO9781107415324.004

Elsayed, G.F., Lara, A.H., Kaufman, M.T., Churchland, M.M., Cunningham, J.P., 2016. Reorganization between preparatory and movement population responses in motor cortex. Nat. Commun. 7. https://doi.org/10.1038/ncomms13239

Eskandar, E.N., Assad, J.A., 2002. Distinct nature of directional signals among parietal cortical areas during visual guidance. J. Neurophysiol. 88, 1777–1790. https://doi.org/10.1152/jn.2002.88.4.1777

Eskandar, E.N., Assad, J.A., 1999. Dissociation of visual, motor and predictive signals in parietal cortex during visual guidance. Nat. Neurosci. 2, 88–93.

Flanagan, J.R., King, S., Wolpert, D.M., Johansson, R.S., 2001. Sensorimotor prediction and memory in object manipulation. Can. J. Exp. Psychol. 55, 87–95. https://doi.org/10.1037/h0087355

Jordan, M.I., Rumelhart, D.E., 1992. Forward models: supervised learning with a distal teacher. Cogn. Sci. 16, 307--354.

Kaas, J.H., Qi, H.X., Stepniewska, I., 2018. The evolution of parietal cortex in primates, Handbook of Clinical Neurology. Elsevier B.V. https://doi.org/10.1016/B978-0-444-63622-5.00002-4

Kaas, J.H., Stepniewska, I., 2016. Evolution of posterior parietal cortex and parietal-frontal networks for specific actions in primates. J. Comp. Neurol. 524, 595–608.

https://doi.org/10.1002/cne.23838
Kang, J.U., Mooshagian, E., Snyder, L.H., 2024. Functional organization of posterior parietal cortex circuitry based on inferred information flow. Cell Rep. 43, 114028. https://doi.org/10.1016/j.celrep.2024.114028
Kaufman, M.T., Churchland, M.M., Ryu, S.I., Shenoy, K.V., 2014. Cortical activity in the null space: Permitting preparation without movement. Nat. Neurosci. 17, 440–448. https://doi.org/10.1038/nn.3643
Li, Y., Wang, Y., Cui, H., 2022. Posterior parietal cortex predicts upcoming movement in dynamic sensorimotor control. Proc. Natl. Acad. Sci. U. S. A. 119, 1–9. https://doi.org/10.1073/pnas.2118903119
Li, Y., Wang, Y., Cui, H., 2018. Eye-hand coordination during flexible manual interception of an abruptly appearing, moving target. J. Neurophysiol. 119, 221–234. https://doi.org/10.1152/jn.00476.2017
Medendorp, W.P., Heed, T., 2019. State estimation in posterior parietal cortex: Distinct poles of environmental and bodily states. Prog. Neurobiol. 183, 101691. https://doi.org/10.1016/j.pneurobio.2019.101691
Merchant, H., Battaglia-Mayer, A., Georgopoulos, A.P., 2003. Interception of real and apparent motion targets: Psychophysics in humans and monkeys. Exp. Brain Res. 152, 106–112. https://doi.org/10.1007/s00221-003-1514-5
Michaels, J.A., Dann, B., Intveld, R.W., Scherberger, H., 2018. Neural dynamics of variable grasp-movement preparation in the Macaque frontoparietal network. J. Neurosci. 38, 5759–5773. https://doi.org/10.1523/JNEUROSCI.2557-17.2018
Michaels, J.A., Dann, B., Intveld, R.W., Scherberger, H., 2015. Predicting reaction time from the neural state space of the premotor and parietal grasping network. J. Neurosci. 35, 11415–11432. https://doi.org/10.1523/JNEUROSCI.1714-15.2015
Mischiati, M., Lin, H.T., Herold, P., Imler, E., Olberg, R., Leonardo, A., 2015. Internal models direct dragonfly interception steering. Nature 517, 333–338. https://doi.org/10.1038/nature14045
Mooshagian, E., Snyder, L.H., 2018. Spatial eye – hand coordination during bimanual reaching is not systematically coded in either LIP or PRR. Proc. Natl. Acad. Sci. U. S. A. https://doi.org/10.1073/pnas.1718267115
Mulliken, G.H., Musallam, S., Andersen, R.A., 2008. Forward estimation of movement state in posterior parietal cortex. Proc. Natl. Acad. Sci. 105, 8170–8177. https://doi.org/10.1073/pnas.0802602105
Nijhawan, R., 1994. Motion extrapolation in catching. Nature 370, 256–257. https://doi.org/10.1038/370256b0
Oristaglio, J., Schneider, D.M., Balan, P.F., Gottlieb, J.P., 2006. Integration of visuospatial and effector information during symbolically cued limb movements in monkey lateral intraparietal area. J. Neurosci. 26, 8310–8319. https://doi.org/10.1523/JNEUROSCI.1779-06.2006
Pachitariu, M., Steinmetz, N., Kadir, S., Carandini, M., Harris, K.D., 2016. Kilosort: realtime spike-sorting for extracellular electrophysiology with hundreds of

channels. bioRxiv 061481.
Port, N.L., Kruse, W., Lee, D., Georgopoulos, A.P., 2001. Motor cortical activity during interception of moving targets. J. Cogn. Neurosci. 13, 306–18.
Rao, R.P.N., 2024. A sensory-motor theory of the neocortex. Nat. Neurosci. https://doi.org/10.1038/s41593-024-01673-9
Sheth, B.R., Nijhawan, R., Shimojo, S., 2000. Changing objects lead briefly flashed ones. Nat. Neurosci. 3, 489–495. https://doi.org/10.1038/74865
Snyder, L.H., Batista, A.P., Andersen, R.A., 2000. Saccade-related activity in the parietal reach region. J. Neurophysiol. 83, 1099–1102. https://doi.org/10.1152/jn.2000.83.2.1099
Snyder, L.H., Batista, A.P., Andersen, R.A., 1997. Coding of intention in the posterior parietal cortex. Nature 386, 167–170. https://doi.org/10.1038/386167a0
So, N., Shadlen, M.N., 2022. Decision Formation in Parietal Cortex Transcends a Fixed Frame of Reference. Neuron 1–10. https://doi.org/10.2139/ssrn.4066028
Subramaniyan, M., Ecker, A.S., Patel, S.S., Cotton, R.J., Bethge, M., Pitkow, X., Berens, P., Tolias, A.S., 2018. Faster processing of moving compared with flashed bars in awake macaque V1 provides a neural correlate of the flash lag illusion. J. Neurophysiol. 120, 2430–2452. https://doi.org/10.1152/jn.00792.2017
Sundberg, K.A., Fallah, M., Reynolds, J.H., 2006. A motion-dependent distortion of retinotopy in area V4. Neuron 49, 447–457. https://doi.org/10.1016/j.neuron.2005.12.023
Witten, I.B., Bergan, J.F., Knudsen, E.I., 2006. Dynamic shifts in the owl's auditory space map predict moving sound location. Nat. Neurosci. 9, 1439–1445. https://doi.org/10.1038/nn1781
Wolpert, D.M., Ghahramani, Z., Jordan, M.I., 1995. An internal model for sensorimotor integration. Science 269, 1880–1882. https://doi.org/10.1126/science.7569931
Zago, M., Bosco, G., Maffei, V., Iosa, M., Ivanenko, Y.P., Lacquaniti, F., 2004. Internal Models of Target Motion: Expected Dynamics Overrides Measured Kinematics in Timing Manual Interceptions. J. Neurophysiol. 91, 1620–1634. https://doi.org/10.1152/jn.00862.2003
Zhang, Y., Chen, Y., Wang, T., Cui, H., 2025. Neural geometry from mixed sensorimotor selectivity for predictive sensorimotor control. eLife 13, 1–21. https://doi.org/10.7554/elife.100064.3
Zheng, C., Wang, Q., Cui, H., 2025. Continuous sensorimotor transformation enhances robustness of neural dynamics to perturbation in macaque motor cortex. Nat. Commun. 16, 1–17. https://doi.org/10.1038/s41467-025-58421-1

667 **Figure**

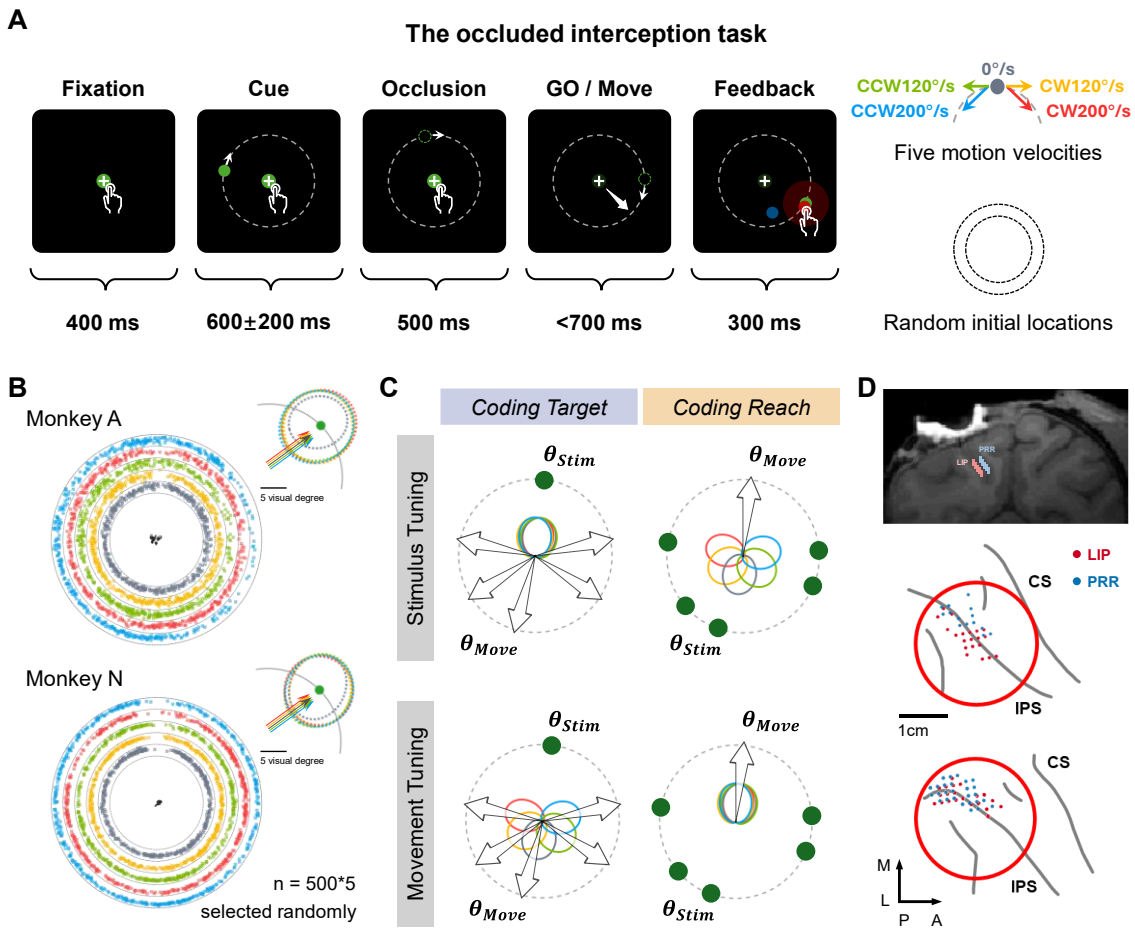

668

669 **Figure 1. Experimental setup and behavioral performance**

670 (A) The occluded interception task. The monkey faced the visual stimuli displayed on a touch
671 screen and interacted with them by hand. A standard trial consisted of five epochs: Fixation,
672 the monkey needed to hold his hand and gaze at the fixation points which denoted by a dot
673 and a cross displaying at the center for 400 ms to start a trial; Cue, a target in the form of a
674 green dot appeared at a random location on the peripheral path (Cue on), the monkey viewed
675 the target, which was either moving or stationary, for 400-800 ms; Occlusion, the target
676 disappeared (Cue off), and the monkey waited for another 500 ms for a signal to move;
677 Go/Move, the central dot was darkened (Go), signaled the monkey to touch the target within
678 700 ms; Feedback, once the monkey touched the screen over 300 ms, the location of both
679 the target and the touch endpoint were displayed, the endpoint was colored red and blue for
680 successful and failed trials, respectively. The velocity of the target was randomly selected
681 from 0 °/s, 120 °/s clockwise (CW) or counterclockwise (CCW), and 200 °/s CW or CCW for

682 each trial. The target path with a radius of 14 visual degree, denoted by the grey dashed
683 circle, was not shown to the monkey. The central dot and cross comprised fixation points to
684 indicate where the gaze and hand needed to hold, respectively, so that the darkness of the
685 dot signified the Go, and the gaze was restricted until the end of the Feedback.
686 (B) The touch and gaze distribution of monkey A (upper) and monkey N (lower) in successful
687 trials. For visualization, the distribution of reach endpoints under each of the five conditions is
688 scaled and displayed separately in annuli arranged in order, with 500 randomly selected trials
689 for each condition. The annulus indicates the tolerance window of 7 visual degree, and insets
690 in the top right show the distribution of motor error, which was calculated by aligning the
691 target to the same location (for example, the location marked by the green dot) after the
692 offset between endpoints and the target was acquired. The colored dots and dashed ellipses
693 indicate the endpoints and 95% confidence interval of motor error in corresponding
694 conditions, respectively. The gaze trajectories in ten randomly selected trials are denoted by
695 black dots around the center, which wander in the tolerance window of 3 visual degree.
696 (C) The hypothetical schematic for distinguishing task-related modulation on single units.
697 Stimulus and movement modulation could be identified by comparing the directional tuning
698 curves defined by target direction (upper row) and reach direction (lower row) across five
699 velocity conditions. Since the reach endpoints were not coupled with specific target locations,
700 the target passing through the same location could lead to reaching movements in various
701 directions (left column), and the movements with the same direction could originate from
702 various target locations (right column). Therefore, a neuron responding to the visual stimulus
703 would show tuning curves directed to the target regardless of the velocity conditions (left
704 column), and a neuron responding to the movement would show tuning curves consistently
705 directed to the reach endpoint (right column).
706 (D) The recording locations. The top panel shows the coronal section that marks the location of
707 the recording chamber. The middle and bottom panels show the lateral view of the right
708 hemisphere of monkey A and monkey N, respectively. Along the intraparietal sulcus (IPS),
709 the estimate of sites for recording LIP and PRR neurons is indicated by red and blue dots,
710 respectively.

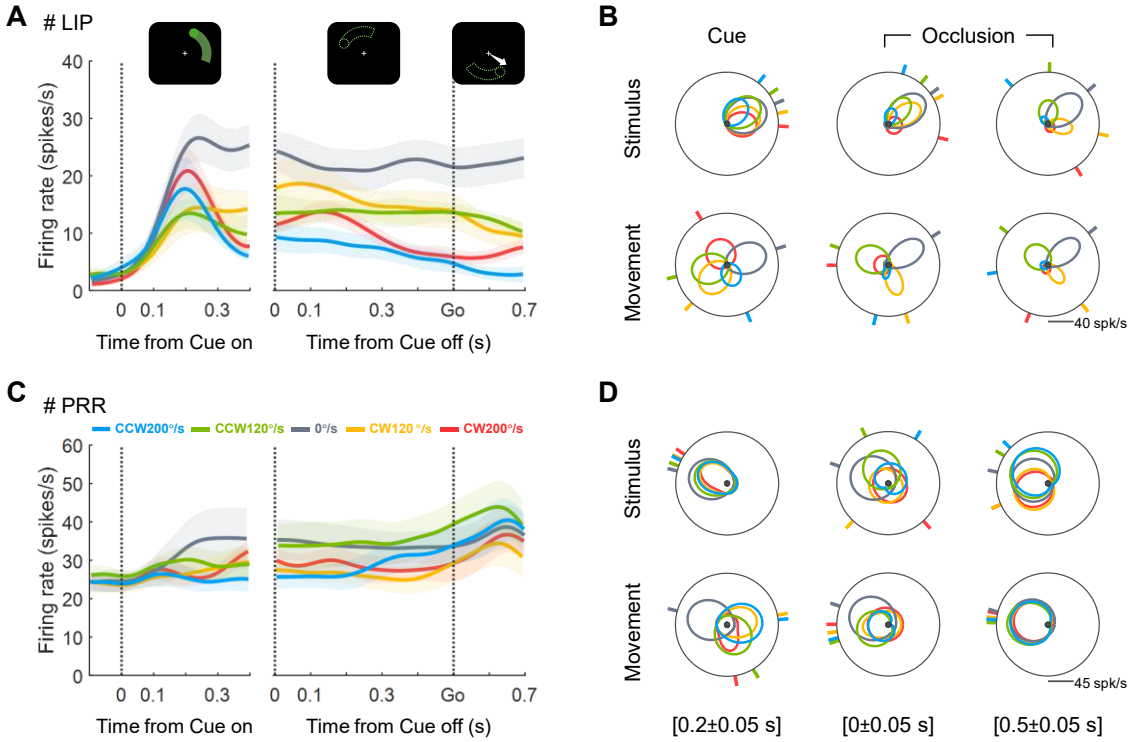

Figure 2. Single-neuron responses during the occluded interception task

(A) Time course of trial-averaged activity for an example LIP neuron. The colored traces represent the firing rates averaged across the trials in the corresponding conditions. The shaded area indicates the standard error. The vertical dotted lines indicate the time point of three events, i.e., Cue on, Cue off, and Go.

(B) The directional tunings of the neuron in (A). The fitted tuning curves and preferred directions (PDs) defined by the direction of real-time stimulus and reaching movement are shown in the upper and lower rows, respectively. From left to right, the tuning curves under five conditions acquired from the time windows centered on 0.2 s after Cue on, Cue off, and Go are denoted by colored petaloid rings, with bars around the circle denoting the corresponding PDs.

(C) Time course of trial-averaged activity for an example PRR neuron.

(D) The direction selectivity of the neuron in (C).

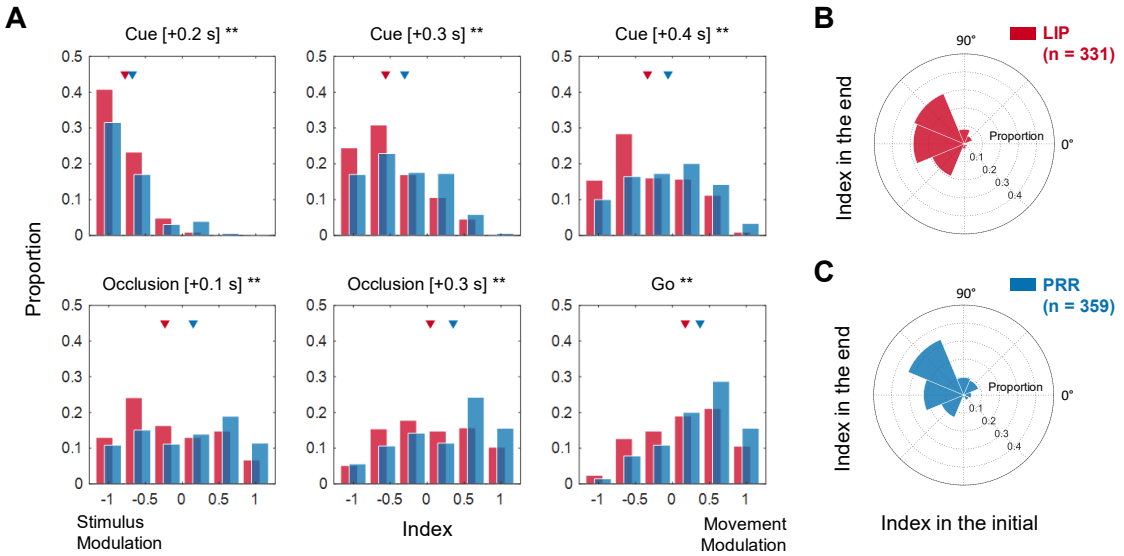

Figure 3. Shift of sensorimotor index in the population of LIP and PRR.

(A) The distributions of sensorimotor index across LIP and PRR neurons are represented by red and blue histograms, respectively. In each time bin, the index was counted only when a neuron demonstrated directional selectivity (i.e., direction-sensitive period). The distributions during the Cue, exemplified as time windows centered on 0.2 s, 0.3 s, and 0.4 s after Cue on, are shown in the upper panels, from left to right. The distributions during the Occlusion, exemplified as time windows centered on 0.1, 0.3 s, and 0.5 s (Go) after Cue off, are shown in the lower panels. The triangles indicate the median of the corresponding distributions, and the asterisks indicate a significant difference in the index distribution between LIP and PRR neurons (Wilcoxon rank sum test; **, $p < 0.01$).

(B) Comparison of the index at the beginning and the end of the direction-sensitive period in LIP neurons. Only the neurons demonstrating directional selectivity over 200 ms were counted, whose shift of the index was indicated by a vector determined by the index in the first and last 50 ms of the period. The distribution was calculated by binning the vectors into 45° zones. The polar histogram pointing to the angle of 135° indicates the fraction of the neurons with the index shift from negative to positive, that is, the neurons displaying sensorimotor transformation.

(C) Comparison of the index in PRR neurons.

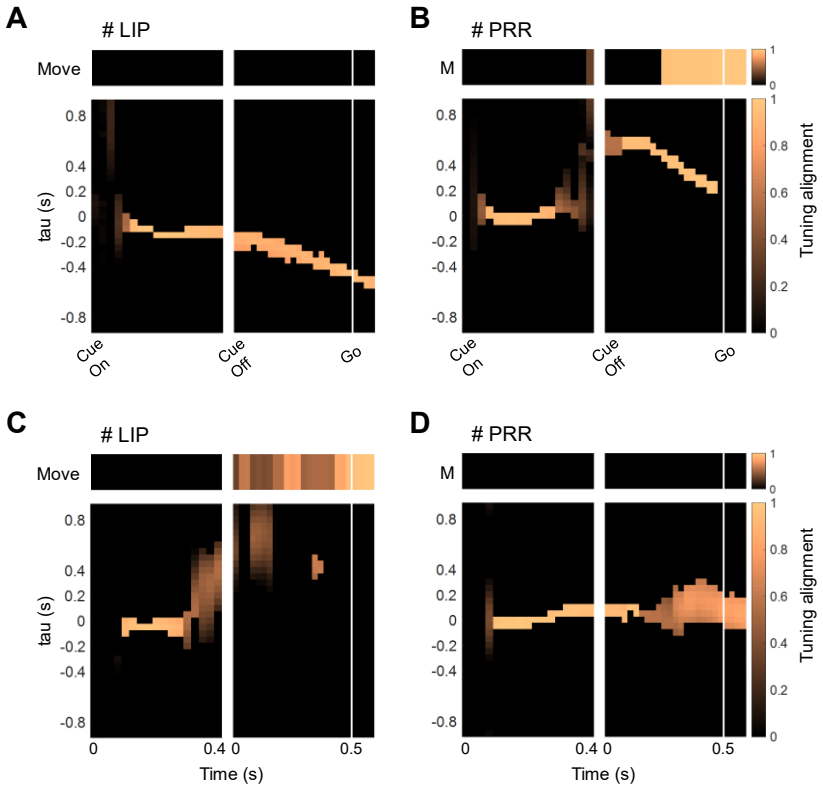

Figure 4. Dynamic tuning states of example neurons.

(A) The tuning states of the example neuron in Figure 2B. In each time window, the possibility of a neuron representing the alternative tuning states was indicated by the alignment of the corresponding directional tunings between conditions. The higher the tuning alignment, the more likely a neuron is to represent that tuning state, and the brighter the corresponding bin. The alternative tuning states include the target states that lead or lag to the actual target, signified by “tau” with a positive or negative value, and the target state at the end of the movement, signified by “Move”. For visualization, only the tuning states with significantly higher tuning alignment were shown.

(B) The tuning states of the example neuron in Figure 2D.

(C) The tuning states of another LIP neuron.

(D) The tuning states of another PRR neuron.

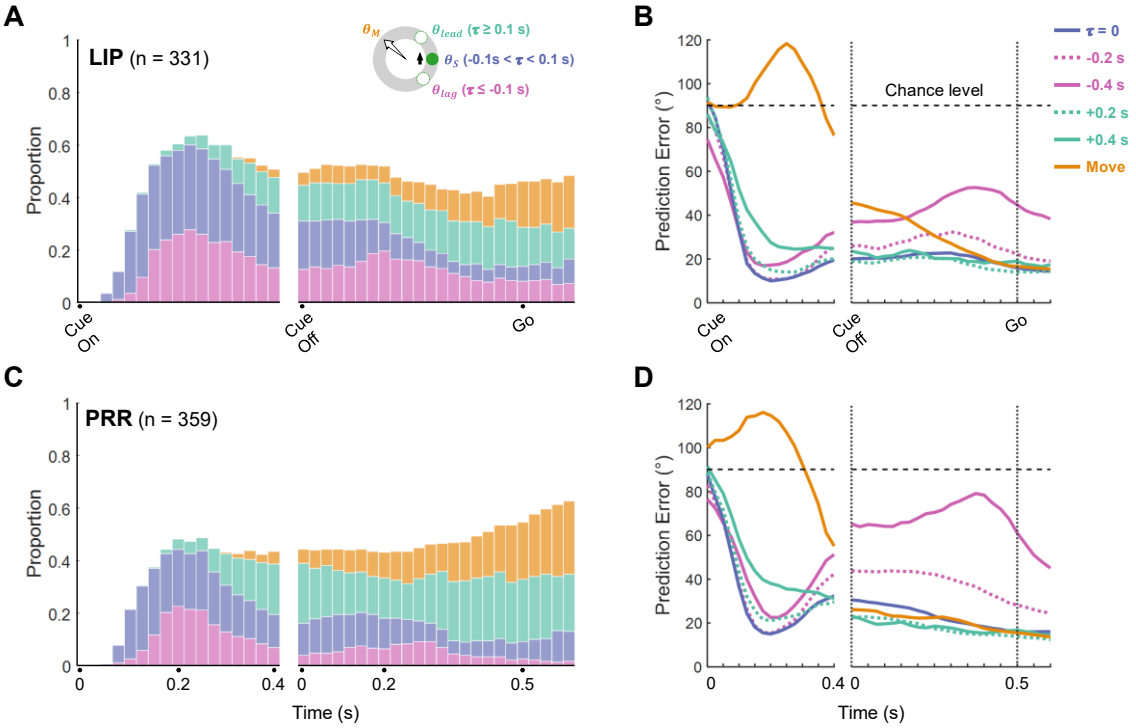

Figure 5. Distribution and read-out of tuning states in the population of LIP and PRR.

(A) The proportion of four kinds of tuning state in LIP neurons across time. According to the relation between the tuning state and the actual target, the tuning states related to the target were sorted into lagging, instantaneous, and leading states, depending on whether the tau is larger than 0.1 s or lower than -0.1 s, whose proportions were indicated by histograms colored pink, purple, and cyan, respectively; the proportion of tuning state related to the intended movement was indicated by the histograms colored orange.

(B) The performance of rSVMs derived from LIP neurons during decoding example tuning states. For each time bin, an rSVM was constructed based on the tuning functions of individual neurons. The instantaneous rSVMs were then tested on the neural data to predict the alternative tuning states. The error in decoding the instantaneous target direction (tau = 0) and reach direction is indicated by the purple and orange lines, respectively. The error in decoding the direction of lagging states with tau of -0.2 s and -0.4 s is indicated by the dotted and solid pink lines, respectively. The error in decoding the direction of leading states with tau of 0.2 s and 0.4 is indicated by the dotted and solid cyan lines, respectively. The horizontal dashed line denotes the chance level of the decoders.

(C) Same as (A), but for PRR neurons.

(D) Same as (B), but for PRR neurons.

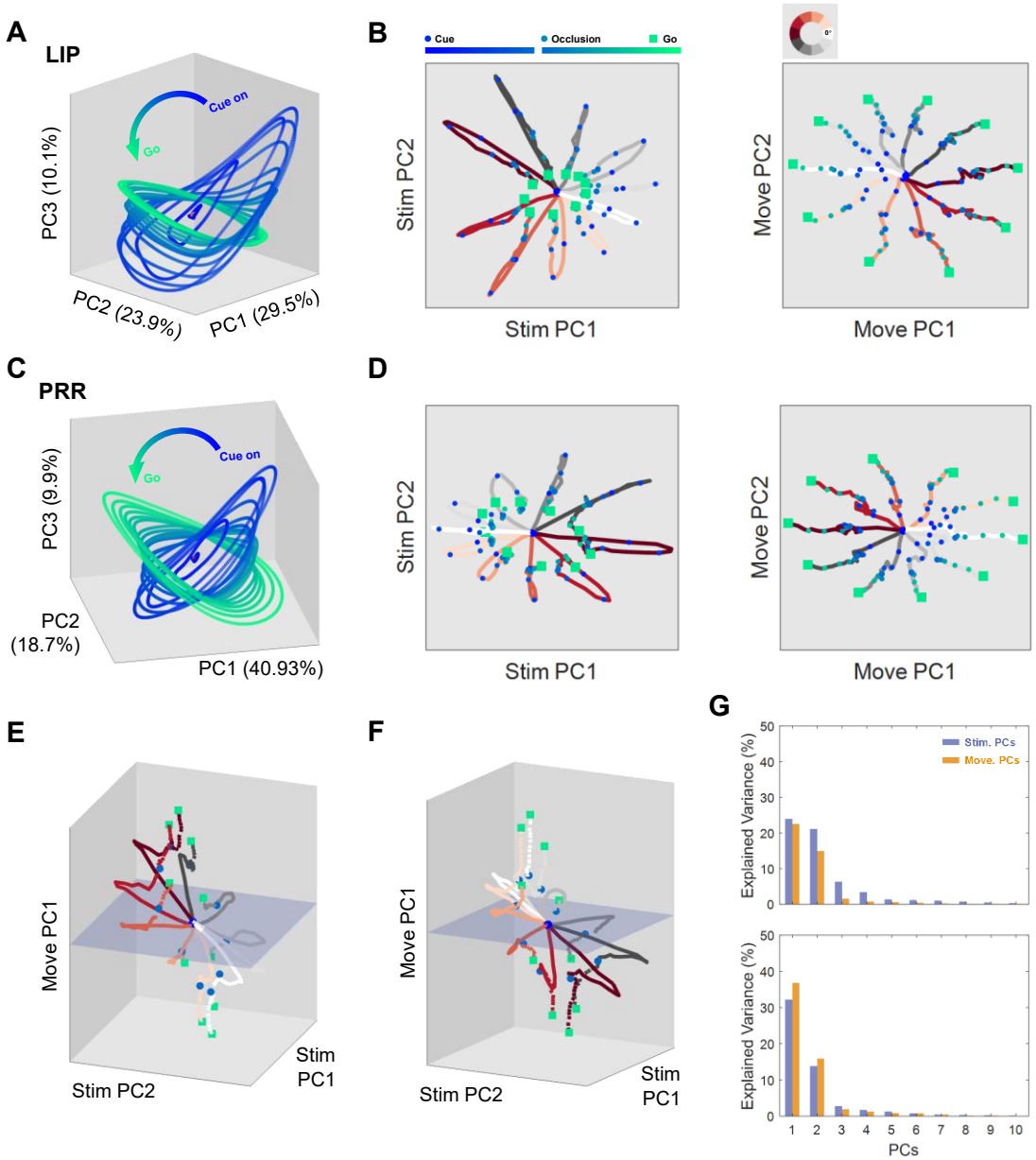

Figure 6. Evolution of the population spatial map in different dimensions.

(A) The three-dimensional view of neural states evolution in the tuning subspace of LIP. The ring consisting of the neural states distributed in directions from 0° to 360° represents the spatial map of the population in one time section. From Cue on to Go with 50 ms interval, the rings colored from blue to green rotated in the low-dimensional space.

(B) The projections of the population spatial map on the dimensions related to stimulus (left) and movement (right) of LIP. The traces colored from red to grey denoted the neural trajectory in ten selected directions, with the time points marked by the dots colored by the same conventions as (A).

(C) The evolution of the spatial map in the tuning subspace of PRR.

(D) The projections of the population spatial map on the stimulus and movement subspace of PRR.

(E) Proportion of the variance in the tuning matrix captured by the top ten stimulus and movement PCs, which was denoted by purple and orange bars, respectively. The data from the population of LIP and PRR was shown in the upper and lower panels, respectively.

(F) The evolution of the spatial map in the space spanned by the first two stimulus PCs and the first movement PC of LIP.

(G) The evolution of the population tuning states

(H) Same as (G), but for data from PRR.

Supplementary figure

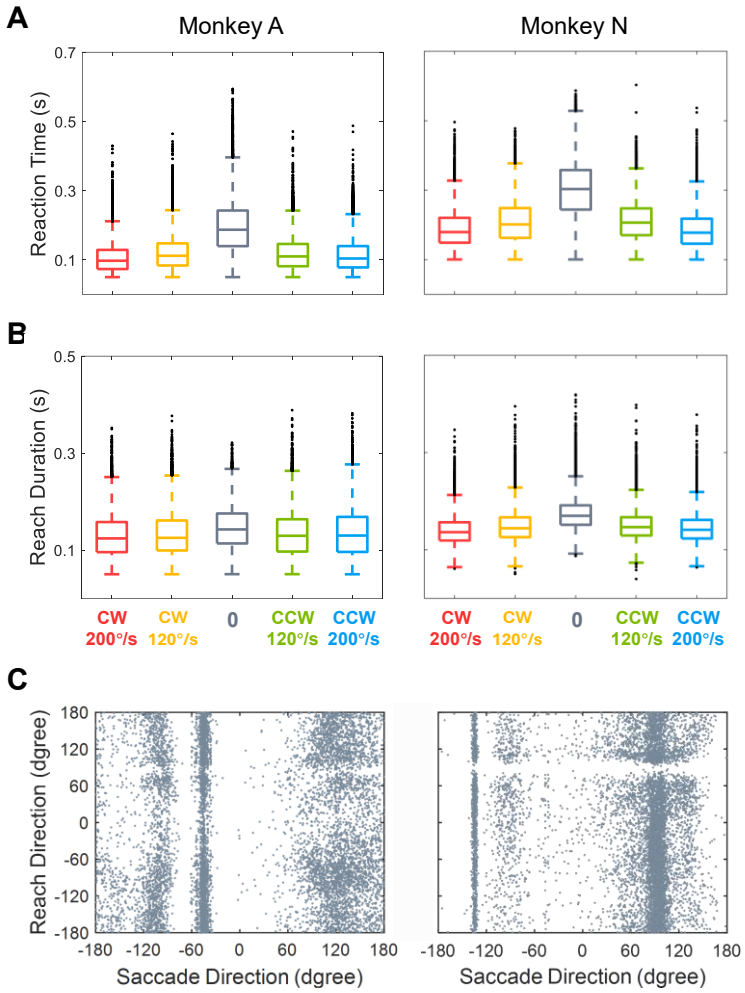

Figure S1. Reaching and saccadic behavioral responses.

(A) The reaction time of monkey A (left) and monkey N (right) in successful trials. From left to right, the distribution in conditions of 200 °/s and 120 °/s CW, 0 °/s, 120 °/s and 200 °/s CCW was shown by the colored box.

(B) The reach duration of monkey A (left) and monkey N (right) in successful trials.

(C) The relationship between the direction of the first saccade after the trial end and reaching movement. Data for demonstration were selected randomly from all successful trials in recording sessions, with 2000 trials for each condition. The correlation between the saccadic and reaching direction was negligible (linear regression, R-square < 0.01, p > 0.1).

807

808 **Figure S2. Trial-averaged responses of the neurons in Figure 2 under different velocity**

809 **conditions and initial regions of the target.**

(A) The schematic for direction grouping. From 0° to 360°, the directions were zoned into eight groups with 45° interval according to the initial location of the target.

(B) The activity of the neuron in Figure 2A when aligning the spike trains to Cue on. The panel in each row displays the neuronal responses in the condition in which the target moved from the zone indicated by (A), with the velocity indicated by color.

(C) Same as (B), but for the neuron in Figure 2B.

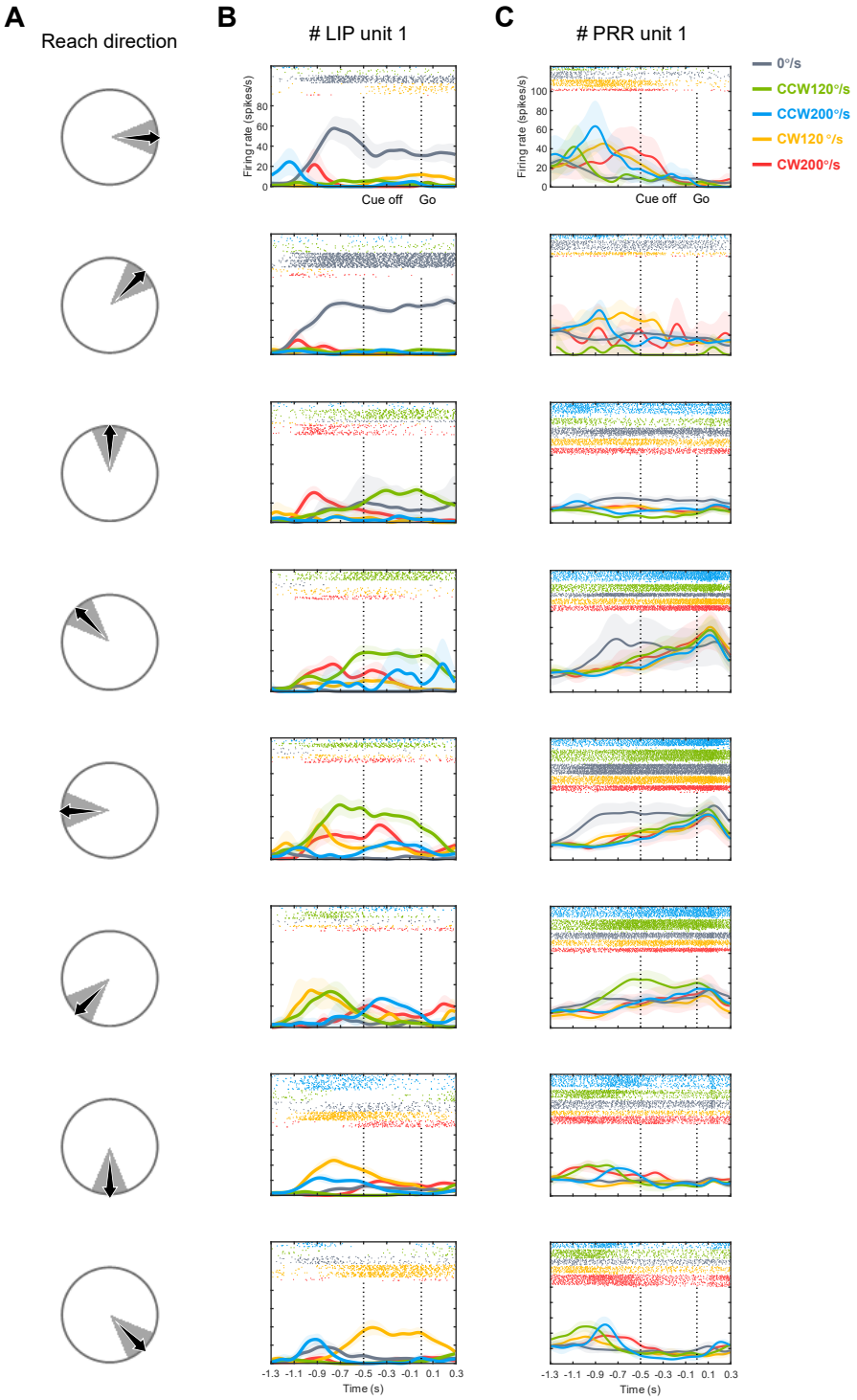

Figure S3. Trial-averaged responses of the neurons in Figure 2 under different velocity conditions and landing regions of reaching movement.

(A) The schematic for direction grouping according to the reach direction.

(B) The activity of the neuron in Figure 2A when aligning the spike trains to Go. The panel in each row displays the neuronal responses in the condition that the reach landing in the zone indicated by (A) to intercept the target moving with the velocity indicated by color.

(C) Same as (B), but for the neuron in Figure 2B.

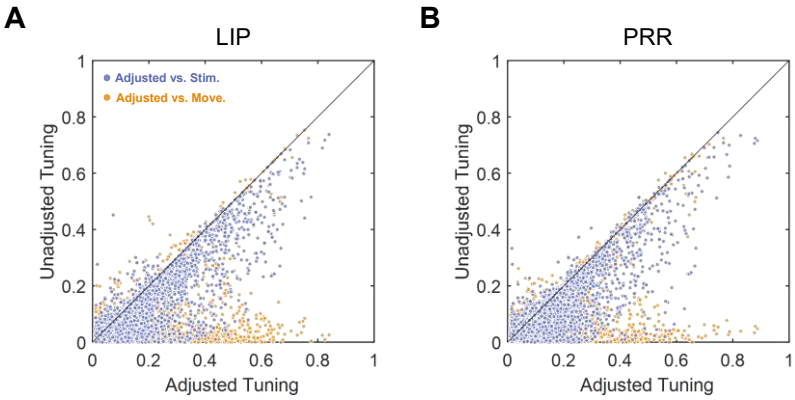

Figure S4. Goodness-of-fit before and after fitting the firing rates with tuning states.

(A) R-square of the directional tunings of LIP neurons, calculated without grouping the trials by conditions. Purple dots represent the comparison between the tunings fitted by the instantaneous target and tuning state, with the R-square of each pair plotted as ordinate and abscissa, respectively. Orange dots represent the comparison between the tunings fitted by the movement and tuning state.

(B) Same as (A), but for PRR neurons.

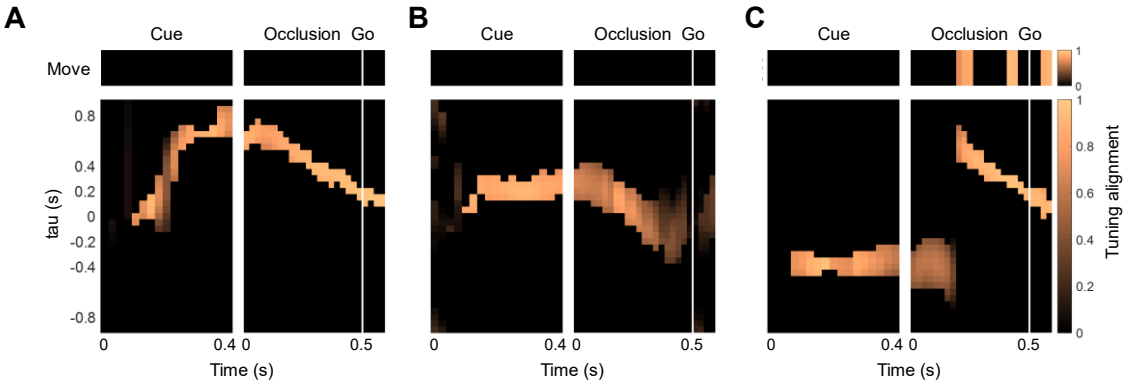

Figure S5. Dynamic tuning states of other neurons.

Same as Figure 5, but for neurons each in (A) monkey N, PRR; (B) monkey A, PRR; (C) monkey A, PRR.

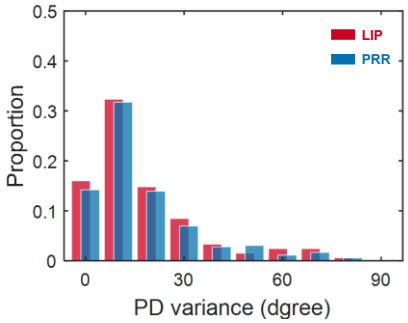

Figure S6. Variance of single neurons' directional selectivity.

The distribution of the variance for preferred direction in the direction-sensitive period. Red and blue histograms represent the variance distribution in LIP and PRR, respectively. Variance was calculated only when a neuron showed directional selectivity over 200 ms.

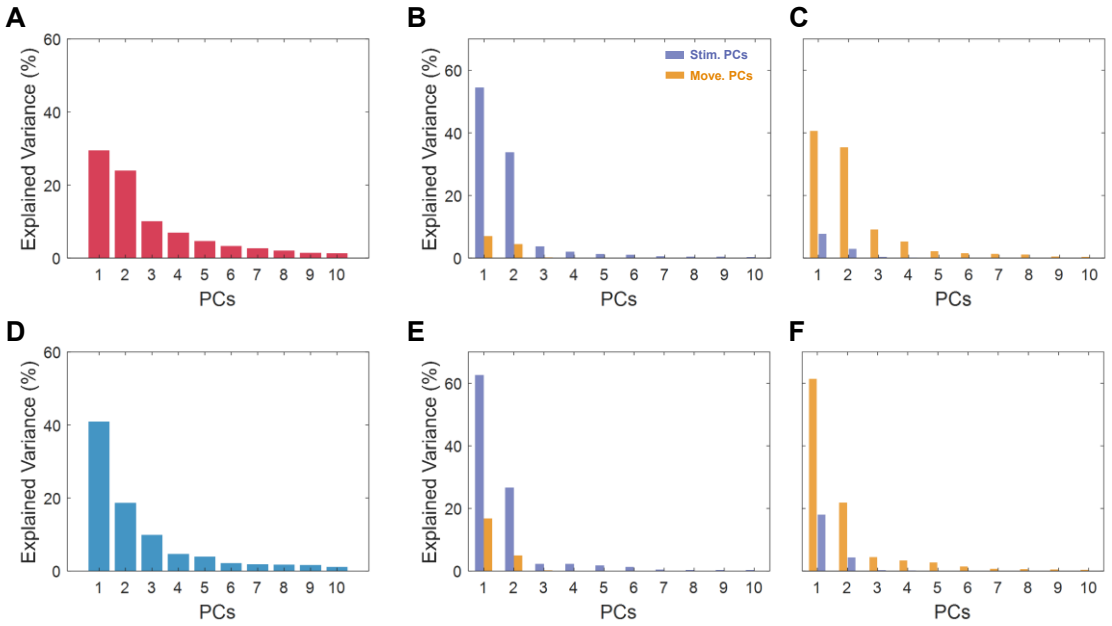

Figure S7. Activity variance explained by the principal components of different subspaces.

(A) Fraction of variance explained by the top ten principal components defined by population tuning data.

(B) For the stimulus-related data, the fraction of variance captured by the top ten principal components of stimulus and movement subspace (Stim-PCs and Move-PCs) is indicated by the purple and orange bars, respectively.

(C) For the movement-related data, the fraction of variance captured by the top ten stimulus and movement principal components.

(D) Same as (A), but for the population activity of PRR.

(E) Same as (B), but for the population activity of PRR.

(F) Same as (C), but for the population activity of PRR.

859 **Table S1. Statistical data of sensorimotor index distribution under six time window.**

		Cue +0.2 s	Cue +0.3 s	Cue +0.4 s	Occlusion +0.1 s	Occlusion +0.3 s	Occlusion +0.5 s / Go
LIP	Skewness	1.45	0.68	0.34	0.29	0	-0.20
	Difference from zero	p<0.001	p<0.001	p<0.001	p<0.001	p=0.07	p<0.001
PRR	Skewness	1.24	0.27	-0.03	-0.18	-0.46	-0.60
	Difference from zero	p<0.001	p<0.001	p=0.01	p=0.05	p<0.001	p<0.001
Difference between areas		p<0.001	p<0.001	p<0.001	p<0.001	p<0.001	p<0.001

860